Continuum finite element analysis of strain localization in slopes

Richard A. Regueiro and Ronaldo I. Borja
Department of Civil Engineering, Stanford University, USA

ABSTRACT: This paper presents a continuum finite element analysis of strain localization in slopes. The stability problem is viewed from the standpoint of strong discontinuity (jump in displacement field) as opposed to weak discontinuity (jump in strain field). For this type of problem, an enhanced finite element solution has previously been shown to be independent of mesh refinement and insensitive to mesh alignment. Numerical simulations of a load-driven slope stability problem in infinitesimal plane strain will demonstrate these characteristics, which are necessary for a finite element solution to be meaningful.

1 INTRODUCTION

Analytical limit equilibrium methods are currently used to analyze slope stability problems where certain simplifying assumptions are made with regard to soil material properties, problem geometry, and shape of slip surface. For complex slope geometries and soil constitutive models, however, analytical limit equilibrium solutions are unwieldy, and the assumption that limit is reached at the load at which a standard finite element (FE) solution fails to converge is unsound. Thus, the need for a more sophisticated numerical tool is in order.

For a FE analysis to be meaningful, it must be objective with respect to mesh refinement and insensitive with respect to mesh alignment (i.e. element sides need not be aligned with the slip surface for the numerical solution to proceed). Both of these characteristics have previously been demonstrated in the context of strong discontinuities (Simo et al. 1993, Simo & Oliver 1994, Armero & Garikipati 1995, Garikipati 1996). A numerical example presented in this paper will demonstrate these attractive qualities of the model.

From the perspective of the practicing geotechnical engineer, post-limit behavior of geotechnical structures is considered useless because the soil has already failed, which is assumed manifest in the formation of a slip surface and in a softening behavior of the soil. In reality, however, the geotechnical structure could contain a slip surface and still be in a pre-limit (pre-collapse) state. Thus, from an analysis standpoint, post-localization behavior should be represented in the model, as long as it is pre-limit. This paper will demonstrate the use of the FE method with strain enhancements to accurately capture slip surfaces in slopes and to predict post-localization behavior, which, it turns out, occurs *before* the standard FE solution fails to converge for a load-driven problem. The critical height of slope predicted by the standard and enhanced FE analyses agrees with that predicted by a simple analytical limit equilibrium analysis. With respect to settlement under a surcharge load at the slope crest, the standard FE solution is shown to be *unconservative* because it predicts a smaller settlement than the enhanced FE solution. In addition, results of the enhanced FE solution motivate the use of the geometrically nonlinear theory. As mentioned above, the usefulness of the FE approximation can be fully realized when conducting numerical slope stability analyses of complex slope geometries and soil constitutive models for which analytical limit equilibrium solutions are unmanageable.

The FE strain enhancements arise naturally from a treatment of classical continuum plasticity with strong discontinuity. It is noteworthy to recognize that the assumption of a discontinuous displacement field leading to a singular strain field

is valid for soils because as a shear band forms between two rigid soil masses sliding along one another, the thickness of the band is negligible (the band reduces to a surface), and the strain across the band approaches infinity (see pictures in Vardoulakis et al. 1978). Important results of the formulation with strong discontinuity are the distributional form of the hardening/softening modulus H, the model-specific stress-displacement relation along the slip surface, and the model-specific localization condition (by "model-specific" it is meant results specific to the classical continuum plasticity model formulated in the context of strong discontinuities). Here, a $J2$ flow plasticity model is formulated in the context of strong discontinuities.

2 $J2$ PLASTICITY WITH STRONG DISCONTINUITY

The following theory is essentially a re-working of that developed by the late Professor Juan C. Simo and his co-workers (Simo et al. 1993, Simo & Oliver 1994, Armero & Garikipati 1995, Garikipati 1996). Also, to keep redundancy to a minimum, reference will be made to the development already given in Borja & Regueiro (1997).

2.1 Review of classical $J2$ plasticity

Before showing the results of the formulation of $J2$ plasticity with strong discontinuities, it is appropriate to review the classical theory. The yield function $\mathcal{F}$ may be written as

$$\mathcal{F}(\boldsymbol{\sigma}) := J_{2D}^2 - \kappa^2 = 0 \qquad (1)$$

where $J_{2D} = \sqrt{\frac{1}{2}\boldsymbol{\sigma}' : \boldsymbol{\sigma}'}$ is the second invariant of the deviatoric Cauchy stress tensor $\boldsymbol{\sigma}'$, and κ is a value constant in stress space used to express the radius $R = \sqrt{2}\kappa = \|\boldsymbol{\sigma}'\|$ of the cylindrical yield surface formed in stress space. An associative flow rule is assumed as

$$\dot{\boldsymbol{\epsilon}}^p = \lambda \hat{\boldsymbol{n}} \qquad (2)$$

where λ is the plastic consistency parameter and $\hat{\boldsymbol{n}} = \boldsymbol{\sigma}'/\|\boldsymbol{\sigma}'\|$ is the unit normal to the yield surface in stress space. The implication of the assumed associative form of the flow rule (i.e. the direction of the plastic flow normal to the yield surface in stress space) is that in order for there to be loss of strong ellipticity of the acoustic tensor, the hardening/softening modulus must be less than or equal

to zero (i.e. perfect of softening plasticity); otherwise, for a nonassociative flow rule, this condition is not necessary (Ortiz et al. 1987).

2.2 Model-specific stress-displacement relation along discontinuity, and localization condition

From the form of the singular part of the plastic consistency parameter, λ_δ, resulting from required regularity (i.e. non-distributional or not singular) of the yield function (Borja & Regueiro 1997), the stress-displacement relation may be written as

$$\begin{aligned} \zeta(t) &= \psi^{-1}\boldsymbol{\sigma}' : \boldsymbol{c}^e : \mathrm{symm}(\boldsymbol{\nabla}\dot{\bar{\boldsymbol{u}}}) ; \\ \psi &= \frac{2\sqrt{2}}{3}\kappa H_\delta \left[\frac{\boldsymbol{\sigma}' : \boldsymbol{c}^e : \mathrm{symm}(\boldsymbol{m} \otimes \boldsymbol{n})}{\boldsymbol{\sigma}' : \boldsymbol{c}^e : \hat{\boldsymbol{n}}} \right] \end{aligned} \quad (3)$$

where $\zeta(t)$ is the magnitude of the jump displacement rate across the discontinuity as a function of time t; $\boldsymbol{c}^e$ is the fourth-order elastic modulus tensor; $\bar{\boldsymbol{u}}$ is the regular part of the displacement vector $\boldsymbol{u}(\boldsymbol{x}, t)$; H_δ is the singular part of the hardening/softening modulus; $\boldsymbol{m}$ is the unit vector denoting the direction of the jump displacement; and $\boldsymbol{n}$ is the unit normal to the discontinuity surface. This expression (3) may be further simplified using results from the localization condition.

From a basic consideration of Newton's third law of motion, we see that the traction across the discontinuity must be continuous (Malvern 1969); also see the discussion by Simo & Oliver (1994) for traction continuity demonstrated in the context of the weak form (variational equation of equilibrium). The model-specific localization condition arises from the satisfaction of this condition that the traction rate be regular on the discontinuity (Armero & Garikipati 1995, Borja & Regueiro 1997). For the case of plane strain this condition may be written as

$$\frac{\|\boldsymbol{\sigma}'\|}{\sqrt{2}|r|} = 1 \quad ; \qquad \theta = \pm 45° \qquad (4)$$

where $r = \frac{1}{2}(\sigma_1 - \sigma_2) = \boldsymbol{n} \cdot \boldsymbol{\sigma} \cdot \boldsymbol{m}$ is the resolved stress along the discontinuity; σ_1 and σ_2 are the major and minor principal stresses ($\boldsymbol{\sigma}$ written in principal stress space); and θ is the angle to the discontinuity normal $\boldsymbol{n}$ from the major principal stress axis. Note that there are two possible directions of $\boldsymbol{n}$ ($\theta = \pm 45°$), a result accounted for in the numerical implementation by choosing the one which aligns the slip surface with the element deformation.

Now, with the results of the localization condition, the model-specific stress-displacement relation (3) representing the softening along the discontinuity surface may be rewritten as

$$r(t) = r(0) + \frac{1}{3} H_\delta \, \alpha(t) \quad ; \quad H_\delta \leq 0 \qquad (5)$$

where $r(0)$ is the resolved stress on the discontinuity at the inception of localization (i.e. satisfaction of (4)), and $\alpha(t)$ is the magnitude of the jump displacement ($\dot{\alpha}(t) = \zeta(t)$, where $\zeta(t)$ is defined in (3)).

3 NUMERICAL IMPLEMENTATION

The finite element formulation begins with a treatment of the standard weak form with strong discontinuities in the context of the assumed enhanced strain method (Simo & Rifai 1990). The discretized form is as follows (Simo & Oliver 1994)

$$\int_\Omega \boldsymbol{\nabla} \bar{\boldsymbol{\eta}}^h : \boldsymbol{\sigma}^h \mathrm{d}\Omega = \int_\Omega \bar{\boldsymbol{\eta}}^h \cdot \boldsymbol{f} \, \mathrm{d}\Omega + \int_{\Gamma_t} \bar{\boldsymbol{\eta}}^h \cdot \boldsymbol{t} \, \mathrm{d}\Gamma$$

$$\int_{\Omega_{e,loc}} \tilde{\boldsymbol{\gamma}}_e^h : \boldsymbol{\sigma}^h \mathrm{d}\Omega = 0 \qquad (6)$$

where $\bar{\boldsymbol{\eta}}^h \in \mathcal{V}^h$ is the regular part of the discretized displacement variation in the space of admissible discretized test functions $\mathcal{V}^h$; $\boldsymbol{f}$ and $\boldsymbol{t}$ are the prescribed body and traction forces, respectively; and $\tilde{\boldsymbol{\gamma}}_e^h \in \tilde{\mathcal{E}}^h$ is the enhanced strain variation in the space of admissible strain variations $\tilde{\mathcal{E}}^h$ over the localized element e with a form chosen to satisfy the patch test (Simo & Rifai 1990). The superscript h denotes finite element discretization. From (6), with the choice of appropriate standard and enhanced shape functions (Borja & Regueiro 1997), the following discretized governing finite element equations result

$$\boldsymbol{R} := \boldsymbol{f}^{\mathrm{ext}} - \mathbb{A}_{e=1}^{n_{el}} \int_{\Omega_e} \boldsymbol{B}_e^T \boldsymbol{\sigma}^h \mathrm{d}\Omega = \boldsymbol{0}$$

$$b_e := -\int_{\Omega_e} \boldsymbol{G}_{\mathrm{patch}}^T : \boldsymbol{\sigma}^h \mathrm{d}\Omega + \int_{S_e} r_S \, \mathrm{d}S = 0 \quad (7)$$

where $\boldsymbol{f}^{\mathrm{ext}}$ is the standard external force vector, $\mathbb{A}_{e=1}^{n_{el}}$ is the finite element assembly operator, $\boldsymbol{B}_e$ is the standard strain-displacement matrix for element e, $\boldsymbol{G}_{\mathrm{patch}}$ is the coupling matrix chosen to ensure satisfaction of the patch test, $r_S = (\int_{\Omega_e} \boldsymbol{n} \cdot \boldsymbol{\sigma}^h \cdot \boldsymbol{m} \mathrm{d}\Omega)/A_e$ is the average resolved stress on the discontinuity, and $\boldsymbol{R}$ and b_e are the corresponding residuals. Note that the governing equation of resolved stress on the discontinuity $(7)_2$

is discontinuous from element to element, which is consistent with the standard C^0 finite element approximation (i.e. the displacements at most must be continuous across element boundaries leading to discontinuous strains). This characteristic of the enhanced strain method is an attractive feature of the model from a numerical implementation standpoint: static condensation of the jump displacement for element e, α_e, may occur at the element level. Equation (7) is consistently linearized to make the equations amenable to solution by the Newton-Raphson method.

4 NUMERICAL EXAMPLE: LOAD-DRIVEN SLOPE STABILITY PROBLEM

To demonstrate the model, a simple load-driven slope stability analysis in infinitesimal plane strain will be performed with the enhanced finite element method discussed in Section 3 and the $J2$ plasticity model with strong discontinuities discussed in Section 2. With such a constitutive model (i.e. deviatoric plastic flow) it is appropriate to model an overconsolidated (significant elastic region) cohesive soil in undrained condition (friction angle $\phi = 0$, zero volumetric plastic flow). Material properties are: modulus of elasticity $E = 10^3$ kPa, Poisson's ratio $\nu = 0.4$, uniaxial yield strength $\bar{\sigma}_o = 40$ kPa, standard hardening/softening modulus $\bar{H} = 0$, hardening/softening modulus along slip surface, $H_\delta = 0$, and saturated unit weight of soil $\gamma = 20$ kN/m^3. The assumed value of the yield strength $\bar{\sigma}_o$ may be interpreted as the failure strength of a cohesive soil with undrained shear strength $c_u = \bar{\sigma}_o/2 = 20$ kPa. For a slope at an angle of 63.43° with c_u and γ as given, an analytical limit equilibrium analysis (Atkinson 1993) predicts a critical height of $H_{cr} \approx 5$ m. Thus, it may be assumed that such a slope with height of 5 m is nearly unstable.

Consider the coarse and fine mesh discretizations of a 5 m high slope at angle 63.43° shown in Figures 1 and 2. The coarse mesh depicted in Figure 1 is composed of 151 nodes and 125 bilinear quadrilateral elements, and the fine mesh consists of 551 nodes and 500 elements. Each mesh is 20 m wide by 10 m high with the crest of the slope at the horizontal center of each mesh. Roller supports are assumed on the two vertical boundaries of each mesh, while the bottom boundary is assumed to be pinned to represent a firm base. The elements were numerically integrated with the $\bar{B}$-

method (2×2 deviatoric, 1-point volumetric) to alleviate mesh locking in the incompressible plastic regime. Points A and B shown in Figure 1 are used on each mesh to calculate the angle of rotation of the slope as it deforms under the surcharge q.
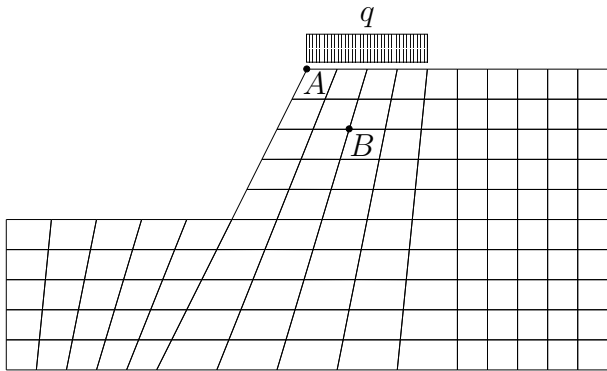

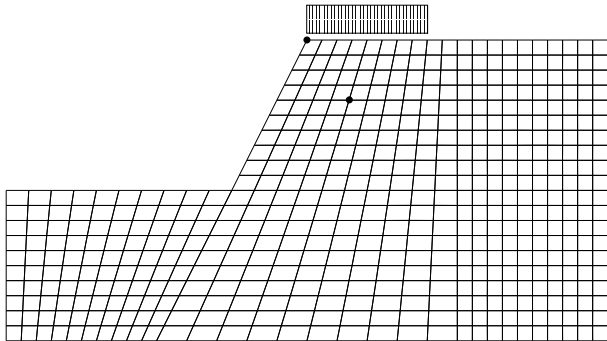Figure 1.   Coarse mesh showing surcharge load and points A and B used to calculate angle of rotation.

Figure 2.   Fine mesh showing surcharge load and points A and B used to calculate angle of rotation (labels left off here).

After application of the gravity load, a surcharge of $q = 14$ kPa at the crest of the slope acting over 4 m is applied to perturb the problem; the small value of q was chosen because at 15 kPa the standard FE solution failed to converge (a uniformly distributed load of this magnitude is equivalent to a 70 cm - thick layer of soil). Along with the result that elements at the slope base begin to localize at the start of surcharge loading, this non-convergence of the standard FE problem at a small surcharge confirms the critical height of 5 m predicted by the analytical limit equilibrium analysis. In addition, when attempting to excavate the first soil layer 1 m deep to the left of the continuous slope line extending through the mesh from the slope crest to the base, both the standard and enhanced FE solutions failed to converge.

Figures 3 and 4 show the deformed coarse mesh at end of surcharge loading for the standard and

enhanced FE solutions, respectively, while Figures 5 and 6 show the same for the fine mesh (magnification factor for displacements = 1.0). The slip surfaces in Figures 4 and 6 are nearly toe circles, which is the shape assumed by the analytical limit equilibrium analysis, and have essentially the same shape for both the coarse and fine meshes, which demonstrates objectivity of the model with respect to mesh refinement. The other characteristic of the finite element model with strain enhancement needed for a numerical analysis to be meaningful—namely, insensitivity to mesh alignment—is easily observed as the slip surface traces across elements not in line with the elements' sides. Note that the elements that have been traced by the slip surface in Figures 4 and 6 have localized according to (4) and thus contain strain enhancement via the enhanced shape functions (Borja & Regueiro 1997) and softening due to plastic flow localized to the discontinuity (see (5) with $H_\delta = 0$). The elements not traced by the slip surface behave according to the standard FE formulation and standard $J2$ plasticity model.
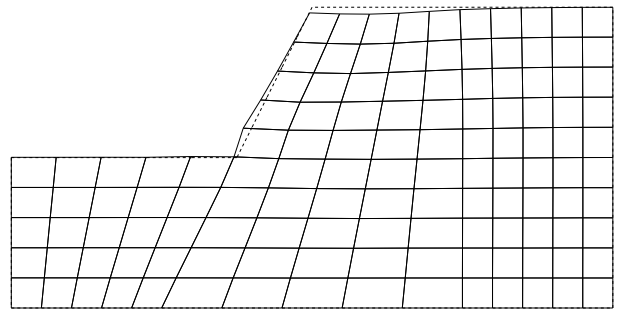

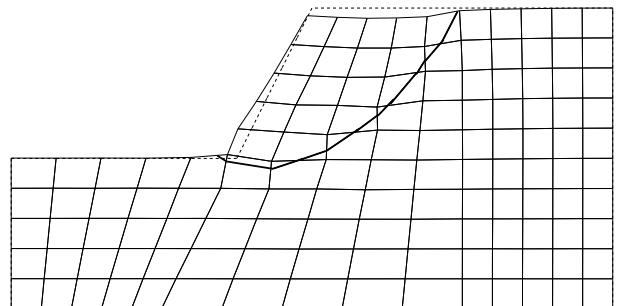Figure 3.   Standard FE solution: coarse mesh at end of surcharge loading.

Figure 4.   Enhanced FE solution: coarse mesh at end of surcharge loading showing slip surface.

To further prove objectivity of the model besides demonstrating similar slip surfaces, a plot of applied surcharge load versus resulting average downward displacement of the top surface of the
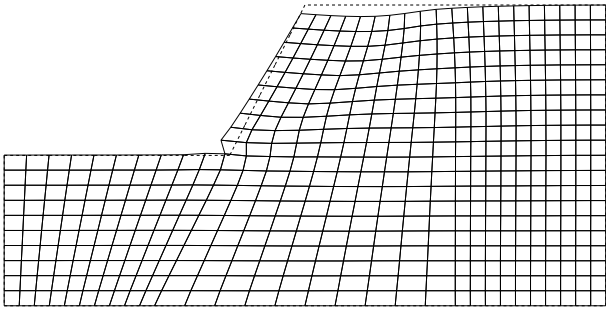
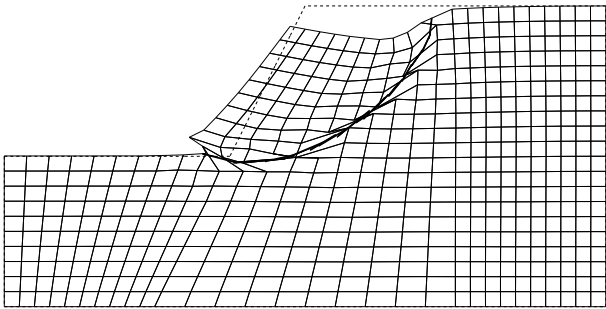Figure 5. Standard FE solution: fine mesh at end of surcharge loading.

Figure 6. Enhanced FE solution: fine mesh at end of surcharge loading showing slip surface.

slope is shown in Figure 7 (Figure 8 is the same plot with abscissa range reduced); and a plot of applied surcharge load versus resulting angle of rotation of point B relative to point A (see Figure 1) is shown in Figure 9 (Figure 10 is the same plot with abscissa range reduced). Note that the displacements and rotations due to the enhanced FE solution for each mesh are in excess of those due to the standard FE solution by approximately the same amount for each load step, demonstrating objectivity with respect to mesh refinement. An already well-known result of the standard FE approximation, the fine mesh shows a softer response than the coarse mesh. As the load steps progress, the enhanced FE solution for both the coarse and fine meshes shows displacements and rotations increasing over those of the standard FE solution, but especially for the fine mesh during the last load step. Such large displacement and rotation at 56 kN/m for the fine mesh shown in Figure 6 motivates the geometrically nonlinear theory (Armero & Garikipati 1996b).

Since this is a load-driven problem, as the load approaches an apparent limit close to 60 kN/m, the FE solutions will eventually not be able to converge, needing a numerical solution method such as an arc-length method to advance the solution. A displacement-driven problem is easier to perform

numerically for this reason, but for problems of interest to the geotechnical engineer, the load-driven problem is more appropriate. On this note, this analysis differs from the one conducted by Armero & Garikipati (1996a).
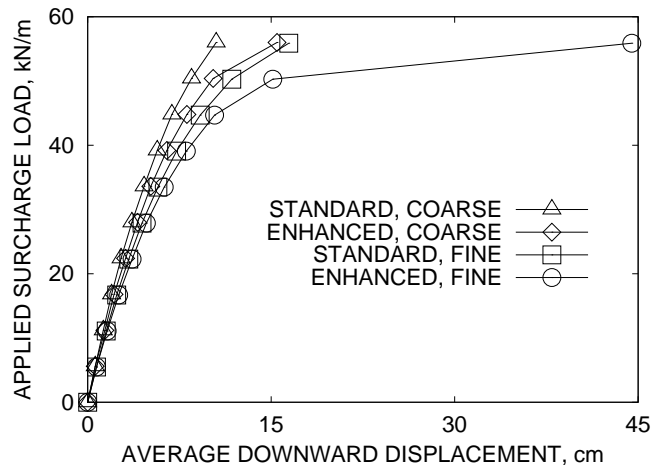

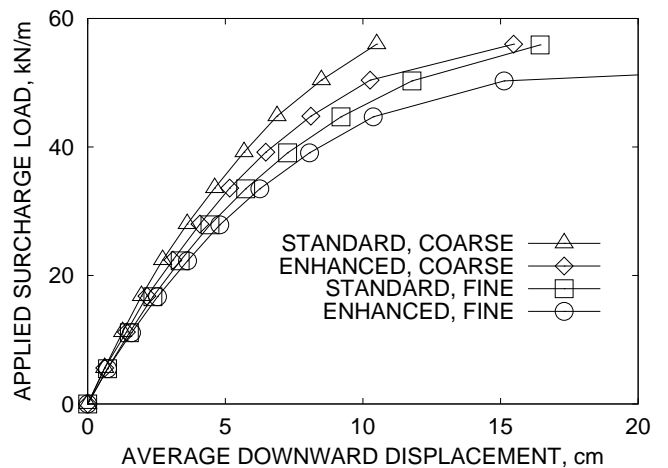Figure 7. Variation of average downward displacement of top surface due to applied surcharge load.

Figure 8. Variation of average downward displacement of top surface due to applied surcharge load (reduced abscissa range).

5 SUMMARY

This paper has demonstrated the usefulness of an enhanced FE method which meets two essential criteria in order for a finite element analysis to be meaningful: objectivity with respect to mesh refinement and insensitivity to mesh alignment. The enhanced FE method has been used to analyze a simple load-driven slope stability problem in order to make a comparison with an analytical limit equilibrium method. The usefulness of the
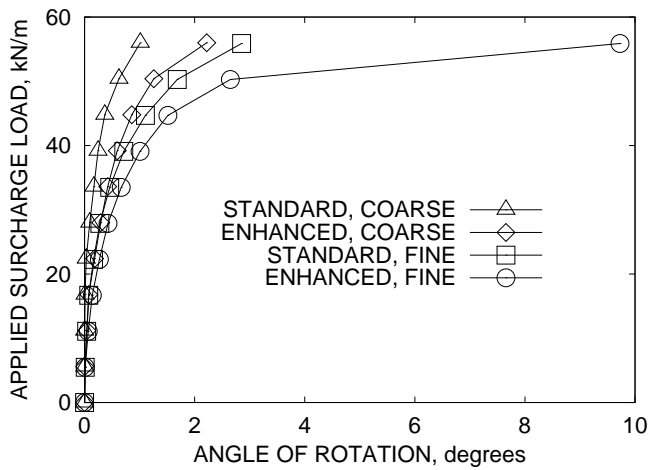
Figure 9. Variation of angle of rotation of point *B* relative to point *A* (see Figure 1) due to applied surcharge load.
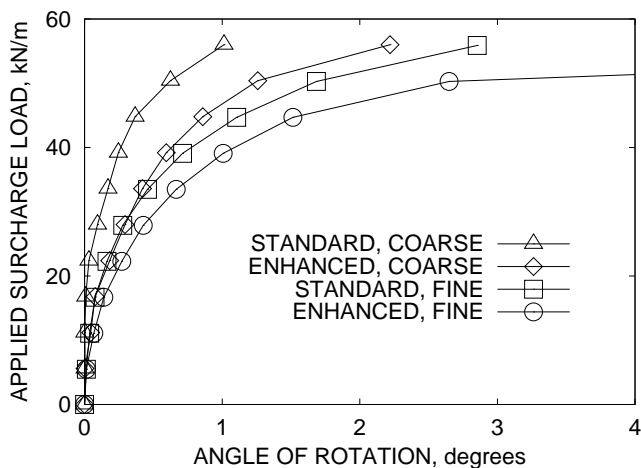

Figure 10. Variation of angle of rotation of point *B* relative to point *A* (see Figure 1) due to applied surcharge load (reduced abscissa range).

model to the practicing geotechnical engineer can be fully utilized when performing numerical slope stability analyses of complex slope geometries involving more complicated soil constitutive models. Work is now in progress to test the model with more appropriate soil constitutive models such as Drucker-Prager and Modified Cam-Clay.

6 ACKNOWLEDGEMENT

REFERENCES

Armero, F. & K. Garikipati 1995. Recent advances in the analysis and numerical simulation of strain localization in inelastic solids. In D.R.J. Owen, E. Onate, & E. Hinton (eds), CIMNE, *Proceedings of Computational Plasticity IV, Barcelona, Spain, April 1995:* 547–561.

Armero, F. & K. Garikipati 1996a. An analysis of strong-discontinuities in inelastic solids with applications to the finite simulation of strain localization problems. In Y.K. Lin & T.C. Su (eds), *Proceedings of 11th Conference on Engineering Mechanics, Fort Lauderdale, FL, May 1996:* 136-139.

Armero, F. & K. Garikipati 1996b. An analysis of strong-discontinuities in multiplicative finite strain plasticity and their relation with the numerical simulation of strain localization in solids. *Int. J. Solids Structures.* 33:2863–2885.

Atkinson, J. 1993. *An introduction to the mechanics of soils and foundations through critical state soil mechanics.* McGraw-Hill.

Borja, R.I. & R.A. Regueiro 1997. Finite element analysis of strain localization in excavations. In F. Oka (ed.), *Proceedings of the International Symposium on Deformation and Progressive Failure in Geomechanics, Nagoya, Japan, October 1997:* in press.

Garikipati, K.R. 1996. *On strong discontinuities in inelastic solids and their numerical simulation.* Ph.D. Dissertation, Stanford University, Stanford, California.

Malvern, L.E. 1969. *Introduction to the mechanics of a continuous medium.* Prentice-Hall: 242.

Ortiz, M., Y. Leroy, & A. Needleman 1987. A finite element method for localized failure analysis. *Comput. Methods Applied Mech. Engrg.*, 61:189–214.

Simo, J.C., J. Oliver, & F. Armero 1993. An analysis of strong discontinuities induced by strain-softening in rate-independent inelastic solids. *Computational Mechanics.* 12:277–296.

Simo, J.C., & J. Oliver 1994. A new approach to the analysis and simulation of strain softening in solids. In Z.P. Bazant, Z. Bittnar, M. Jirasek, & J. Mazars (eds), *Fracture and Damage in Quasibrittle Structures.*

Simo, J.C., & M.S. Rifai 1990. A class of mixed assumed strain methods and the method of incompatible modes. *Int. J. Num. Methods in Engrg.* 29:1595–1638.

Vardoulakis, I., M. Goldschieder, & G. Gudehus 1978. Formation of shear bands in sand bodies as a bifurcation problem. *Int. J. Num. Anal. Methods Geomech.* 2:99–128.